Indium interaction with the $Bi_2Se_3(0001)$ surface under the low-temperature deposition

© S.A. Ponomarev[1,2], D.I. Rogilo[1,2], V.A. Golyashov[1], D.A. Nasimov[1], K.A. Kokh[3], D.V. Sheglov[1], A.V. Latyshev[1,2]

[1] Rzhanov Institute of Semiconductor Physics, Siberian Branch, Russian Academy of Sciences, 630090 Novosibirsk, Russia
[2] Novosibirsk State University, 630090 Novosibirsk, Russia
[3] V.S. Sobolev Institute of Geology and Mineralogy of the Siberian Branch of the RAS, 630090 Novosibirsk, Russia

E-mail: ponomarev@isp.nsc.ru

Received December 5, 2024
Revised December 6, 2024
Accepted December 6, 2024

The adsorption of indium atoms on the $Bi_2Se_3(0001)$ surface at room temperature followed by annealing at 200°C was studied using *in situ* reflection electron microscopy, angle-resolved photoelectron spectroscopy and X-ray photoelectron spectroscopy. The formation of a heterostructure in the form of a Bi(111) bilayer on the $Bi_2Se_3(0001)$ surface and the formation of an In−Se chemical bond, which corresponded to the emergence of bismuth atoms on the surface from the near-surface layer with the next formation of a Bi(111) islands were shown. Regions with an increased indium content surrounded by labyrinthine bismuth islands without pronounced step faceting were observed by scanning electron microscopy in the backscattered electron mode. Bismuth islands Bi(111) with a height of ≈ 0.4 nm were also observed by atomic force microscopy.

Keywords: indium, $Bi_2Se_3(0001)$, bilayer, replacement of atoms, *in situ* REM, AFM, XPS, ARPES.

DOI: 10.61011/SC.2024.11.59955.18S

1. Introduction

Materials with van der Waals (VDW) gap, in particular layered metal chalcogenides, are promising for photovoltaics, photonics, and electronics applications [1–5]. A specific feature of representatives of this class of materials is the presence of a variety of structural polymorphs — a material with the same stoichiometry can have a variety of crystal structures with different electronic and optical properties [5–7]. In this case, according to the first reviews dealing with the study of layered metal chalcogenides [1,8], the presence of a weak VDW gap between layers should have provided the possibility to obtain layered heterostructures with any necessary properties by alternating two-dimensional (2D) layers of different VDW materials and (or) their polymorphic modifications similar to the blocks of „Lego“ constructor, regardless of the crystal structure of the VDW substrate.

However, attempts to obtain high-quality layers of VDW materials by such epitaxy methods as, for example, chemical vapour deposition (CVD) and molecular beam epitaxy (MBE) have revealed a number of problems involving a high concentration of structural defects formed both at the initial stages and during the growth of layered heterostructures [5,9,10]. In addition to defect formation, the possibility of diffusion, for example, of indium atoms adsorbed from the molecular beam into the depth of the substrate of layered Bi_2Se_3 with subsequent substitution of bismuth atoms was also pointed out in some studies, which affected the mobility of carriers [11], or even caused the Bi_2Se_3 layer to turn into β-In_2Se_3 [12] due to the similarity of their crystal structure (lattice parameters of $a = 4.12$ Å, $c = 28.48$ Å and $a = 3.99$ Å, $c = 28.31$ Å respectively) [12–14]. The high-temperature adsorption of an indium sub-monolayer coating (> 400°C) onto the $Bi_2Se_3(0001)$ surface with simultaneous deposition of a selenium molecular beam was also previously demonstrated, leading to the formation and growth of an impurity-induced 2D indium phase with a height of 0.4 nm [15], which locally suppressed the sublimation of the underlying Bi_2Se_3 layer resulting in the formation of star-shaped multilayer islands after sublimation of several layers. The results of the above-mentioned works do not provide complete information on the process of interaction of indium with the surface of $Bi_2Se_3(0001)$ at low temperatures (below the sublimation temperature of Bi_2Se_3 ≈ 400°C) and its influence on the subsequent growth of In_2Se_3/Bi_2Se_3 heterostructures. Moreover, the available literature still lacks information on the changes in the band structure of the $Bi_2Se_3(0001)$ surface upon interaction with indium which makes the combined application of *in situ* and *ex situ* research methods necessary.

This paper contains the results of *in situ* and *ex situ* investigations of the interaction of indium atoms with the surface of $Bi_2Se_3(0001)$ deposited at room temperature followed by annealing at 200°C. The experiments show the substitution of bismuth atoms by adsorbed indium atoms in the near-surface layer, which led to the formation of local areas of the indium-containing phase $InSe_x$ covered with a

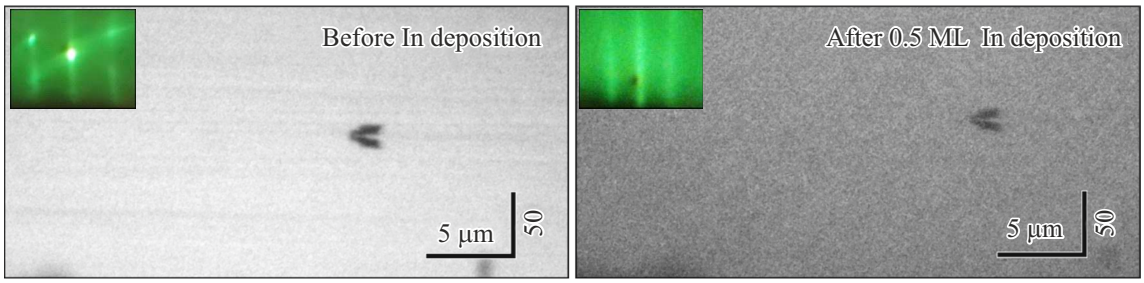

Figure 1. REM images of the surface before indium deposition and after ≈ 0.5 ML indium deposition, top left of the REM images of the surface — insets of the reflected high energy electron diffraction (RHEED) patterns corresponding to the surface before and after 0.5 nm indium deposition.

bismuth bilayer Bi(111) with a height of 0.4 nm, formed due to the exit of substituted bismuth atoms to the surface.

2. Experimental and measuring technique

To study the adsorption of indium onto the surface of $Bi_2Se_3(0001)$ in the *in situ* reflection electron microscopy (REM) column, samples with dimensions of $7 \times 3 \times 0.3$ mm obtained by exfoliation from a single crystal of Bi_2Se_3 grown by the Bridgman [16,17] method were used. Exfoliation was carried out under atmospheric conditions followed by cutting the edges. Indium of 99.999% purity (Ted Pella, USA) and selenium of 99.999% purity (Metallon, Russia) were used as deposition materials. The indium evaporator was calibrated by the rate of formation of surface reconstruction $\sqrt{3} \times \sqrt{3}$ at 450°C on the pre-annealed Si(111) surface, according [18–20].

The chemical composition and electronic structure of the sample surface were investigated by X-ray photoelectron spectroscopy (XPS) and angle-resolved photoelectron spectroscopy (ARPES). Measurements were performed on a SPECS photoelectron spectrometer equipped with a ASTRAIOS-190 hemispherical electron energy analyser with an electrostatic deflector, using monochromatised AlK_α ($h\nu = 1486.7$ eV) radiation for XPS and non-monochromatised HoI_α ($h\nu = 21.22$ eV) radiation for ARPES. Indium was deposited on the $Bi_2Se_3(0001)$ surface by electron beam evaporation from a molybdenum crucible, and the deposition rate was monitored using quartz microbalance and by XPS. Observation of the surface atomic structure change was carried out by means of low-energy electron diffraction (LEED).

After the experiments, the samples were studied by atomic force microscopy (AFM, Bruker, Multimode 8) and scanning electron microscopy (SEM, Hitachi SU8220).

3. Experimental results and discussion

To clean the surface of the $Bi_2Se_3(0001)$ sample from contaminants and crystal particles formed on the surface due to exfoliation under atmospheric conditions, annealing at 450°C under vacuum conditions ($\sim 10^{-7}$ Pa) with simultaneous deposition of selenium (≈ 0.1 nm/s) for 10 min — under these conditions, congruent sublimation with preservation of the surface morphology [21] was observed. Then, to study the adsorption of indium on the $Bi_2Se_3(0001)$ surface ≈ 0.5 ML indium (1 ML ≈ 0.2 nm) deposition experiments were performed at a rate of ≈ 0.01 nm/s at room temperature of the substrate followed by annealing at 200°C in the absence of selenium flux to the surface. Reflection high energy electron diffraction (RHEED) and reflectance electron microscopy (REM) techniques were used to *in situ* diagnose the processes on the sample surface. The deposition of ≈ 0.5 ML indium on the $Bi_2Se_3(0001)$ surface at room temperature and subsequent annealing at 200°C led to a decrease in the intensity of the RHEED pattern and terrace contrast on electron microscopic images (Figure 1), which indicates the structural and morphological transformation of the surface.

Similar *in situ* experiments were carried out in the ARPES chamber at a residual pressure $5 \cdot 10^{-8}$ Pa and indium deposition rate ≈ 0.008 nm/s. In Figure 2, *a* and *d* the band dispersion pattern obtained by the ARPES method for the clean surface of the $Bi_2Se_3(0001)$ in the M−Γ−M direction close to the Γ-point of the surface Brillouin zone is presented and its curvature [22], which allows us to highlight the main details in the obtained spectrum. Below the Fermi level, the electronic states of the bulk conduction band with a parabolic dispersion law (E_c) and the surface states of the topological insulator with a quasi-linear Dirac spectrum (TSS) are visible. The Dirac point of the topological surface states is located 0.3 eV below the Fermi level — close to the top of the bulk valence band states (E_v). The deposition of 1 ML indium at room temperature leads to a significant broadening of the lines in the ARPES spectra (Figure 2, *b* and *e*), but all spectral features characteristic of the Bi_2Se_3 surface remain distinguishable. One can also notice a shift of all features in the spectra toward higher binding energies by approximately 0.1 eV, which may be related to a change in the band bending on the surface or additional electron doping of the surface due to the adsorption of indium atoms. Subsequent heating of the sample at 200°C for 30 min in ultrahigh vacuum leads to significant changes in

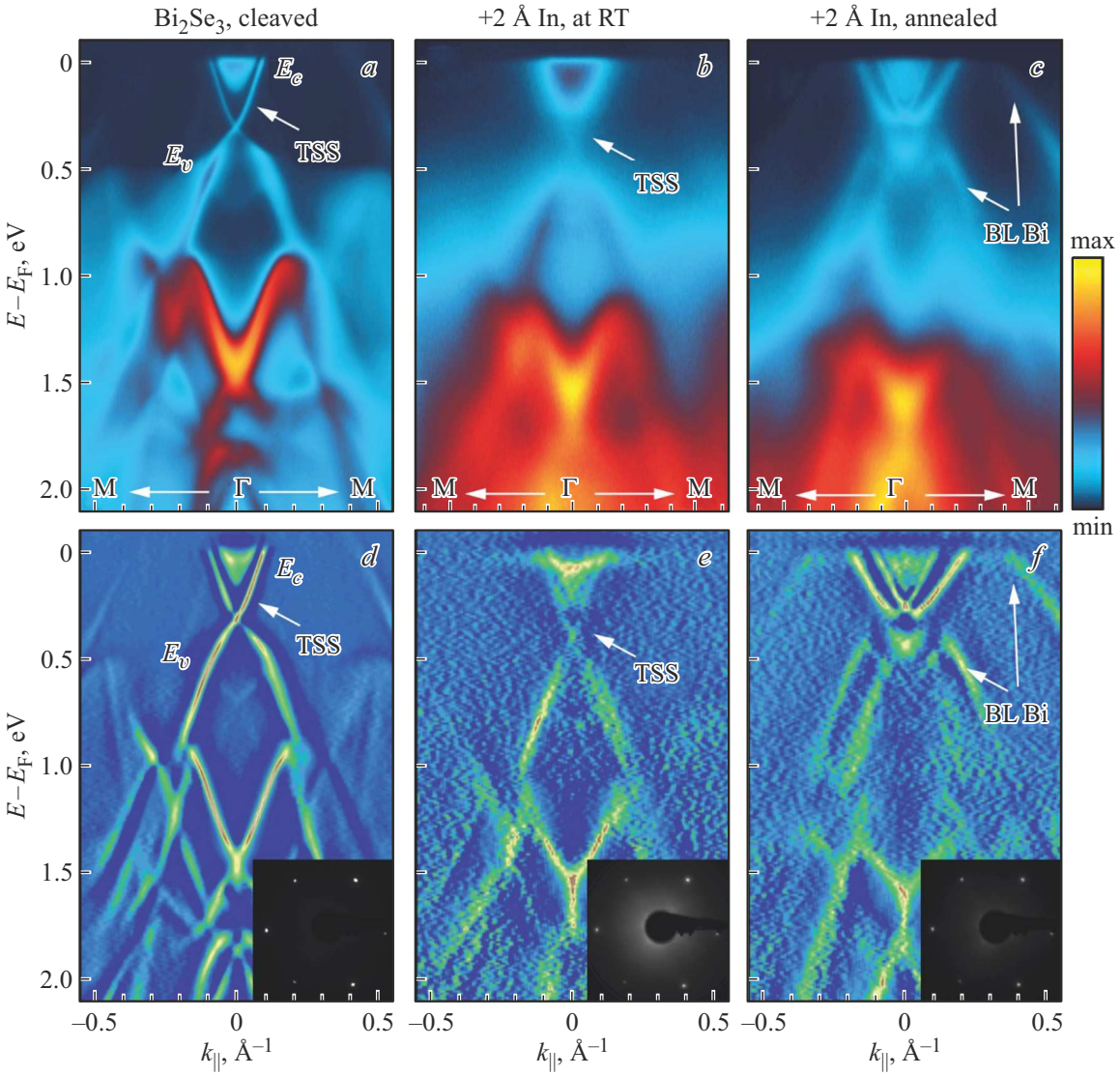

Figure 2. The ARPES spectra of the $Bi_2Se_3(0001)$: surface: *a* — after chipping in vacuum, *b* — deposition of ≈ 2 Å indium at room temperature, *c* — subsequent heating of the sample at 200°C. *d*–*f* — the corresponding curvature patterns of the ARPES spectra shown in *a*–*c*. Measurements were made in the M–Γ–M direction of the Brillouin zone of the $Bi_2Se_3(0001)$ surface at 80 K, $h\nu = 21.22$ eV. The insets show the corresponding LEED patterns measured at an electron beam energy of 39 eV. (A color version of the figure is provided in the online version of the paper).

the observed electronic structure of the surface (Figure 2, *c* and *f*). Near the Γ-point, electronic states with strong Rashba splitting appear. A new set of hole states also appears: with a parabolic dispersion law crossing the Fermi level at $k_{||} = \pm 0.4$ Å^{-1}and M-shaped near the Γ-point at binding energies > 0.45 eV. This pattern is broadly similar to the spectrum of states of the bismuth Bi(111) bilayer on the $Bi_2Se_3(0001)$ [23–25] surface.

To study the effect of In atoms adsorption on the chemical composition of the $Bi_2Se_3(0001)$ surface, the XPS method was used. Figure 3 shows the changes in the XPS spectra of the In3*d*, Bi4$d_{7/2}$ and Se3*d* lines of the $Bi_2Se_3(0001)$ spallation surface after deposition of an In layer of thickness ≈ 2 Å at room temperature and subsequent heating of the sample at 200°C. The values of the XPS bond energies of the Bi4$f_{7/2}$ and Se3$d_{5/2}$ lines for the pure $Bi_2Se_3(0001)$ surface are 157.83 and 53.34 eV respectively. As previously observed in the XPS spectra, the deposition of In atoms leads to a shift of all observed photoemission lines in the direction of higher bond energies by 0.14 eV. The bond energy of the In3$d_{3/2}$ lines is 452.08 eV, which is ≈ 0.7 eV higher than the value expected for metallic indium in the In0 oxidation state ($E_b = 451.39$ eV) [26], and means that after deposition all indium atoms are chemically bonded to selenium atoms on the Bi_2Se_3 surface. In addition, a broadening of the Se_{3d} line and the appearance of an additional Bi4$f_{7/2}$ line component with a binding energy of 157 eV corresponding to the appearance of bismuth atoms in the Bi0 state are observed. It can be assumed that the deposition of indium atoms on the surface of Bi_2Se_3

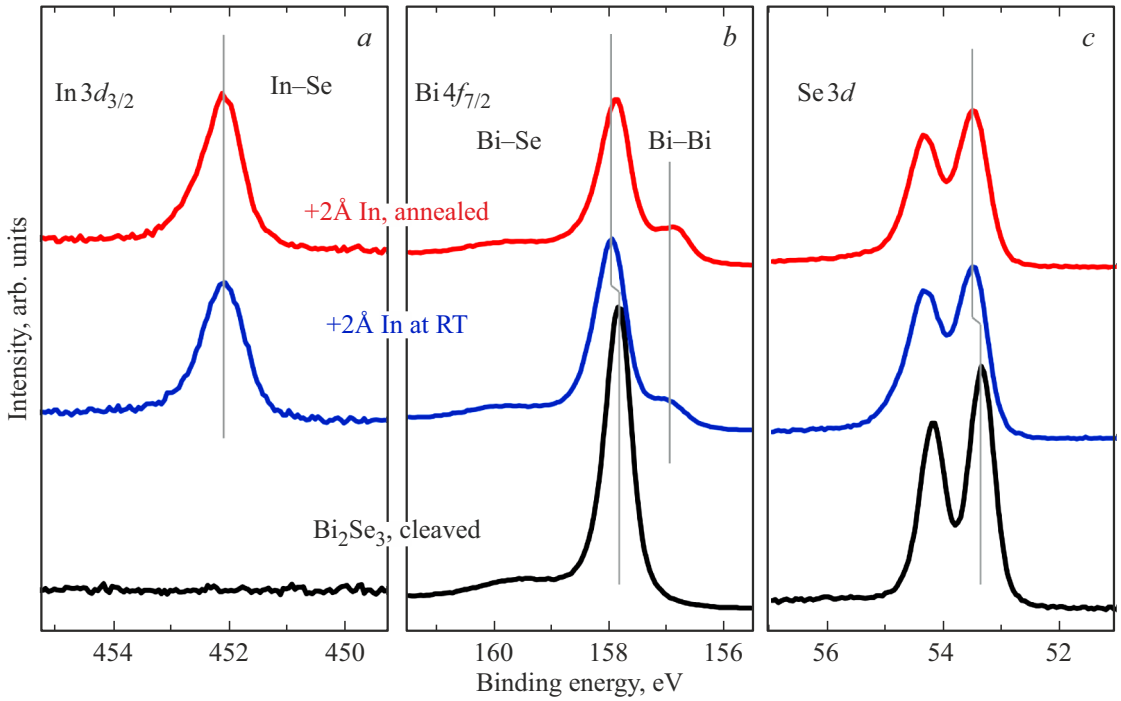

Figure 3. XPS spectra of In3*d* (*a*), Bi4$d_{7/2}$ (*b*) and Se3*d*, lines measured for a pure $Bi_2Se_3(0001)$ surface after spalling in vacuum (black lines), after deposition of ≈ 2 Å indium at room temperature (blue lines) and subsequent sample heating at 200°C.

at room temperature leads to the substitution of bismuth atoms for indium atoms in the near-surface pentalayer of Bi_2Se_3 and the formation of amorphous clusters Bi on its surface. Estimation of the effective thickness of this surface layer of elemental bismuth from the ratio of the intensities of the Bi−Bi and Bi−Se components of the Bi4$f_{7/2}$ line gives the value ≈ 2 Å. Additional heating of the sample leads to an increase in the effective thickness of the Bi surface layer to ≈ 2.9 Å; this value is close to the thickness of the bismuth bilayer (3.9 Å) and corresponds to a coverage of about 3/4 of the substrate surface area Bi_2Se_3. Thus, based on the XPS data, the deposition of indium atoms and additional annealing of the sample leads to the formation of a heterostructure in the form of Bi(111) bilayers on the Bi_2Se_3 surface with individual $InSe_x$ phase inclusions. In LEED patterns, a decrease in the intensity of diffraction spots was observed after deposition of In atoms on the Bi_2Se_3 surface and subsequent annealing, but the hexagonal (1×1) diffraction pattern of the unreconstructed $Bi_2Se_3(0001)$ surface was always preserved. Unfortunately, it was not possible to identify the features of the electronic and atomic structure containing indium from the photoemission measurements. However, since there is no decrease in the intensity of the XPS lines of In when the structures are heated, it can be stated that there is no diffusion of indium atoms deep into the substrate or formation of a solid solution $(Bi_{1-x}In_x)_2Se_3$.

After the measurements by *in situ* REM, XPS and ARPES methods, AFM analysis of the surface morphology showed that there were no significant differences in the surface morphology of the samples obtained in the *in situ* REM column and the ARPES unit, indicating that the experimental conditions were the same. In Figure 4, *a* an image of the surface morphology of the samples after deposition of 1 ML indium is shown, in which a two-dimensional labyrinth-like layer without pronounced faceted boundaries can be seen with a height of ≈ 0.4 nm, occupying ∼ 60% of the area. Taking into account the results of ARPES and XPS, this corresponds to the ∼ 1 ML surface segregation of bismuth atoms from the near-surface layer and the formation of a Bi(111) bilayer 0.4 nm high and occupying about half of the surface area of the [25].

For SEM analysis of the $Bi_2Se_3(0001)$ surface, a sample coated with ∼ 0.5 ML of indium was used, which was insufficient to replace bismuth atoms in the near-surface layer over the entire surface, leaving localised areas of the original surface that had not been transformed due to interaction with indium. Figure 4, *b* shows a SEM image of the surface obtained using a backscattered electron detector, whose signal carries information about the *Z*-contrast (areas with a higher content of elements with a high charge number *Z* have a brighter contrast). It can be seen that domains with a height of 0.4 nm (according to the AFM measurements), marked with white arrows, have a bright contrast, which corresponds to an increased concentration of bismuth atoms, heavier than selenium and indium atoms. These domains are located around the darker regions marked with black arrows, in which the near-surface bismuth atoms are replaced by indium atoms but are not covered by the Bi(111) bilayer. The area occupied by the light and dark contrast is about half of the area of the whole surface image. The rest of the image is occupied by regions of contrast with intermediate

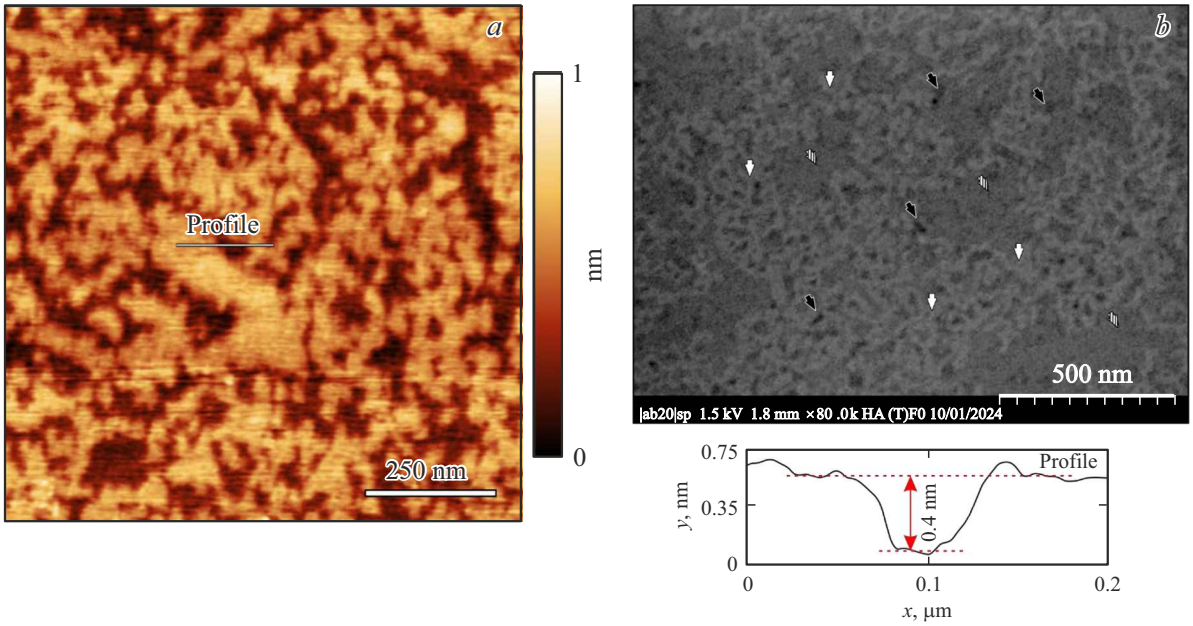

Figure 4. *a* — AFM image of the Bi_2Se_3 surface after deposition of indium with 0.4 nm high Bi(111) bilayers. *b* — SEM image of the surface in the backscattered electron mode: white arrows indicate regions corresponding to Bi(111) bilayers, black arrows — regions of the surface reacted with indium but not covered by the Bi(111) bilayer, shaded arrows — regions with the original surface $Bi_2Se_3(0001)$.

intensity, marked by shaded arrows and corresponding to the $Bi_2Se_3(0001)$ surface, which was not transformed in the experiment due to insufficient amount of deposited indium. Such regions have an intermediate contrast compared to the areas darker due to indium content and the labyrinth-shaped layer lighter due to increased bismuth concentration. Thus, the totality of the results obtained by AFM, SEM, XPS and ARPES methods indicates the substitution of bismuth atoms by indium atoms in the near-surface layer with their subsequent aggregation on the surface in the form of a two-dimensional bilayer.

4. Conclusion

Experiments on the adsorption of indium onto the surface of $Bi_2Se_3(0001)$ at room temperature followed by annealing at $\approx 200^\circ$C have been carried out using *in situ* REM, ARPES and XPS. It was found that indium deposition already at room temperature leads to the substitution of Bi atoms in the Bi_2Se_3 near-surface layer by In atoms. During subsequent annealing at $\approx 200^\circ$C the bismuth atoms displaced to the surface form a Bi(111) bilayer having a labyrinth-like morphology without pronounced faceting of the boundaries and a height of 0.4 nm.

Funding

Experiments on the study of indium adsorption on the surface of $Bi_2Se_3(0001)$ by the *in situ* methods of REM, AFM, XPS and ARPES were carried out with the financial support of the Russian Science Foundation (grant No. 22-72-10124). Diagnostics by SEM method was supported by the Russian Science Foundation (grant No. 19-72-30023). This study was carried out using the equipment of the CRF „Nanostructures“. The single crystal $Bi_2Se_3(0001)$ used for sample preparation was obtained by the Bridgman method within the framework of the state order IGM SB RAS 122041400031-2.

Conflict of interest

The authors declare that they have no conflict of interest.

References

[1] S. Vishwanath, X. Liu, S. Rouvimov, L. Basile, N. Lu, A. Azcatl, K. Magno, R.M. Wallace, M. Kim, J.-C. Idrobo, J.K. Furdyna, D. Jena, H.G. Xing. J. Mater. Res., **31** (7), 900 (2016).
[2] F. Wang, Y. Zhang, Y. Gao, P. Luo, J. Su, W. Han, K. Liu, H. Li, T. Zha. Small, **15** (30), 1901347 (2019).
[3] F. Xia, H. Wang, D. Xiao, M. Dubey, A. Ramasubramaniam. Nature Photonics, **8** (12), 899 (2014).
[4] G. Fiori, F. Bonaccorso, G. Iannaccone, T. Palacios, D. Neumaier, A. Seabaugh, S.K. Banerjee, L. Colombo. Nature Nanotechnol., **9** (10), 768 (2014).
[5] A. Giri, G. Park, U. Jeong. Chem. Rev., **123** (7), 3329 (2023).
[6] L. Liu, J. Dong, J. Huang, A. Nie, K. Zhai, J. Xiang, B. Wang, F. Wen, C. Mu, Z. Zhao, Y. Gong, Y. Tian, Z. Liu. Chem. Mater., **31** (24), 10143 (2019).
[7] J. Wu, Z. Hu, Z. Jin, S. Lei, H. Guo, K. Chatterjee, J. Zhang, Y. Yang, B. Li, Y. Liu, J. Lai, R. Vajtai, B. Yakobson, M. Tang, J. Lou, P.M. Ajayan. Adv. Mater. Interfaces, **3** (16), 1600383 (2016).
[8] A.K. Geim, I.V. Grigorieva. Nature, **499** (7459), 419 (2013).

[9] S. Vishwanath, P. Dang, H.G. Xing. Molec. Beam Epitaxy, 443 (2018).
DOI: https://doi.org/10.1016/B978-0-12-812136-8.00017-7
[10] Y. Nie, A.T. Barton, R. Addou, Y. Zheng, L.A. Walsh, S.M. Eichfeld, R. Yue, C.R. Cormier, C. Zhang, Q. Wang, C. Liang, J.A. Robinson, M. Kim, W. Vandenberghe, L. Colombo, P.-R. Cha, R.M. Wallace, C.L. Hinkle, K. Cho. Nanoscale, **10** (31), 15023 (2018).
[11] H.D. Lee, C. Xu, S.M. Shubeita, M. Brahlek, N. Koirala, S. Oh, T. Gustafsson. Thin Sol. Films, **556**, 322 (2014).
[12] W.E. McMahon, C.L. Melamed, H. Zhang, J.L. Blackburn, P. Dippo, A.C. Tamboli, E.S. Toberer, A.G. Norman. J. Cryst. Growth, **573**, 126306 (2021).
[13] X. Chen, H.D. Zhou, A. Kiswandhi, I. Miotkowski, Y.P. Chen, P.A. Sharma, A.L. Lima Sharma, M.A. Hekmaty, D. Smirnov, Z. Jiang. Appl. Phys. Lett., **99** (26), 261912 (2011).
[14] N. Balakrishnan, C.R. Staddon, E.F. Smith, J. Stec, D. Gay, G.W. Mudd, O. Makarovsky, Z.R. Kudrynskyi, Z.D. Kovalyuk, L. Eaves, A. Patané, P.H. Beton. 2D Mater., **3** (2), 025030 (2016).
[15] S.A. Ponomarev, D.I. Rogilo, D.A. Nasimov, K.A. Kokh, D.V. Sheglov, A.V. Latyshev. J. Cryst. Growth, **628**, 127545 (2024).
[16] K.A. Kokh, Y.M. Andreev, V.A. Svetlichnyi, G. V. Lanskii, A.E. Kokh. Cryst. Res. Technol., **46** (4), 327 (2011).
[17] K.A. Kokh, S. V. Makarenko, V.A. Golyashov, O.A. Shegai, O.E. Tereshchenko. CrystEngComm, **16** (4), 581 (2014).
[18] S.A. Ponomarev, K.E. Zakhozhev, D.I. Rogilo, A.K. Gutakovsky, N.N. Kurus, K.A. Kokh, D.V. Sheglov, A.G. Milekhin, A.V. Latyshev. J. Cryst. Growth, **631**, 127615 (2024).
[19] A. Zotov, A. Saranin, O. Kubo, T. Harada, M. Katayama, K. Oura. Appl. Surf. Sci., **159–160**, 237 (2000).
[20] S. Ponomarev, D. Rogilo, A. Mironov, D. Sheglov, A. Latyshev. 2021 IEEE 22nd Int. Conf. of Young Professionals in Electron Devices and Materials. EDM, **2021** (18), 50 (2021).
[21] S.A. Ponomarev, D.I. Rogilo, N.N.N. Kurus, L.S. Basalaeva, K.A. Kokh, A.G.G. Milekhin, D. V. Sheglov, A. V. Latyshev. J. Phys.: Conf. Ser., **1984**, 012016 (2021)
[22] P. Zhang, P. Richard, T. Qian, Y.-M. Xu, X. Dai, H. Ding. Rev. Sci. Instrum., **82** (4), 043712 (2011).
[23] L. Miao, Z.F. Wang, W. Ming, M.-Y. Yao, M. Wang, F. Yang, Y.R. Song, F. Zhu, A.V. Fedorov, Z. Sun, C.L. Gao, C. Liu, Q.-K. Xue, C.-X. Liu, F. Liu, D. Qian, J.-F. Jia. Proc. Natl. Acad. Sci., **110** (8), 2758 (2013).
[24] T. Lei, K.-H. Jin, N. Zhang, J.-L. Zhao, C. Liu, W.-J. Li, J.-O. Wang, R. Wu, H.-J. Qian, F. Liu, K. Ibrahim. J. Phys. Condens. Matter, **28**(25), 255501 (2016).
[25] S.H. Su, P.Y. Chuang, S.W. Chen, H.Y. Chen, Y. Tung, W.C. Chen, C.H. Wang, Y.W. Yang, J.C.A. Huang, T.R. Chang, H. Lin, H.T. Jeng, C.M. Cheng, K.D. Tsuei, H.L. Su, Y.C. Wu. Chem. Mater., **29** (21), 8992 (2017).
[26] Alexander V. Naumkin, Anna Kraut-Vass, Stephen W. Gaarenstroom, Cedric J. Powel. NIST *X*-ray Photoelectron Spectroscopy Database, NIST Standard Reference Database Number 20, National Institute of Standards and Technology [(Gaithersburg MD, 20899 (2000)].

Translated by J.Savelyeva